Depression of vibronic levels and transition from the dynamic to static Jahn-Teller effect in the $^4T_1$ multiplet: The case of Co^{2+} in ZnSe

S. M. Uba and J. M. Baranowski
Institute of Experimental Physics, Warsaw University, 00-681 Warsaw, Poland
(Received 12 November 1976)

A complete comparison between experimental absorption due to the $^4A_2(F)-^4T_1(F)$ transition of substitutional Co^{2+} in ZnSe and theoretical predictions based on the Jahn-Teller model is presented. An exact numerical solution of the full Hamiltonian, in which spin-orbit interaction and Jahn-Teller coupling are included, is in very good agreement with the energy position and intensities of the observed absorption lines. It is shown that the predominant Jahn-Teller coupling is with the low-frequency mode of $\hbar\omega = 72$ cm^{-1} of E symmetry, which originates from the peak of the density of states of the transverse-acoustic phonons of ZnSe. The frequency of this Jahn-Teller active mode coupled to the lowest electronic level of the $^4T_1(F)$ term is drastically reduced by the second-order Jahn-Teller interaction within the $^4T_1(F)$ term. The analytic expressions and numerical calculations for the depression of vibronic levels in the case of E- and T_2-mode coupling are presented and discussed. It is shown that for the $^4T_1(F)$ state the depression of vibronic levels is almost the same in the case of E-mode and T_2-mode coupling. Finally, it is shown that the $^4T_1(F)$ state of Co^{2+} in ZnSe is suffering the Jahn-Teller effect in the region of transition between the dynamic and static effect.

I. INTRODUCTION

It has been known for some time that fine structures of crystal-field spectra of ions in solids are not explained by static crystal-field theory. The dynamic Jahn-Teller (JT) effect offered the possibility of explaining often very complicated experimental data. It is known that electron-phonon interaction can strongly influence the fine-structure splittings of crystal-field spectra.

It was shown by Ham[1] that strong JT coupling may in certain circumstances drastically reduce the spin-orbit splittings expected for crystal-field theory. Good examples of such reduction were observed in the $^4T_2$ term of V^{2+} and Co^{2+} in $KMgF_3$ by Sturge[2,3] and recently in $^4T_1$ terms of Mn^{2+} in ZnS, ZnSe, and CdS by Koidl.[4]

However, Ham's theory is based on the condition that the JT interaction is large compared to the spin-orbit splitting which is not likely to be met in II-VI compound semiconductors doped with impurities of relatively large spin-orbit interaction. The opposite case of weak coupling is more probable, when the JT energy is smaller or comparable to the spin-orbit splitting. The weak JT coupling has been found to prevail in the $^5T_2$ term of Fe^{2+} in MgO,[5] ZnS,[6] and $CdIn_2S_4$,[7] and in the $^2T_2$ term of Cu^{2+} in ZnS, CdS, and ZnO.[8] Later, it was shown that the $^4T_2$ and $^4T_1(F)$ terms[9,10] of Co^{2+} and the $^3T_1(P)$ term[11] of Ni^{2+} in ZnS fall in this category. The important feature of weak JT coupling, which was noticed by Ham *et al.*,[5,6] Koidl *et al.*,[9,11] Ryskin *et al.*,[10] Maier, and Sauer *et al.*,[12,13] is that it may produce a drastic depression of the lowest vibronic levels.

The optical absorption spectra of substitutional Co^{2+} in II-VI and III-V compounds have been studied by several authors.[9,10,14-25] The optical absorption of Co^{2+} in ZnSe has been also studied previously.[18] The interpretation of the ZnSe:Co spectrum has been done up to now only in the frame of static crystal-field theory.[18]

In this work we present detailed absorption data concerning the fine structure of the $^4T_1(F)$ term in ZnSe:Co with full interpretation of all details. Our interpretation follows the way described by Ham *et al.*[5,6] and recently developed by Koidl *et al.*[9]

However, our calculations go beyond a mere fit to the observed spectrum of Co^{2+} in ZnSe. Although the numerical calculations presented in this work were done for values of spin-orbit parameter, crystal-field parameters, and the energy of JT active mode most suitable for ZnSe:Co, it is possible to extend them and to obtain some general conclusions.

This was possible to do owing to the improvement of our program which permits inclusion of a large number of phonon-coupled states up to $N = 20$ for the E mode as compared to Koidl's[9] $N = 4$. Such a large number of phonon-coupled states allowed us to improve significantly the accuracy of our calculations. The effect of depression of vibronic levels could be calculated exactly for the E mode in a wide range of JT energy. It was possible to show that the mechanism of depression of vibronic levels leads finally to static distortion. Thus, an approach to the static JT effect in the weak-coupling scheme was now possible for the first time.

The analytical expressions for depression of

vibronic levels in the case of E mode and T_2 mode, as well, are derived. It is also shown that in the $^4T_1(F)$ state suffering JT distortion due to coupling to the T_2 mode, the vibronic energy levels and intensities of optical transitions to them are remarkably similar to the case of coupling to the E mode.

II. EXPERIMENTAL

The spectra were observed from cubic ZnSe with Co impurities introduced to the melt. The spectra were measured on a Cary 17 spectrophotometer. The sample was immersed in liquid helium which was pumped to 1.5 K.

The absorption band due to $^4A_2(F)$-$^4T_1(F)$ transition within the $3d^7$ shell of the Co^{2+} impurity being substitutional on zinc site is shown in Fig. 1. The energies of the strongest lines relative to the zero-phonon line are given on the drawing.

III. STATIC CRYSTAL-FIELD THEORY

The energy-level scheme of Co(d^7) in a cubic environment, resulting from the ^4F and ^4P atomic states is well known. The ground state of Co(d^7) being on substitutional cation site is $^4A_2(F)$. The spin-allowed optical transitions from the $^4A_2(F)$ state to the $^4T_2(F)$, $^4T_1(F)$, and $^4T_1(P)$ excited quartets are responsible for the characteristic absorption spectrum of Co(d^7).

In this work we are mainly concerned with details of the $^4A_2(F)$-$^4T_1(F)$ absorption band. However, the full interpretation of this spectrum requires knowledge of crystal-field parameter Δ, Racah parameters B and C, and spin-orbit parameter ζ. The Δ and B parameters can be determined from the baricenters of absorption to the $^4T_2(F)$, $^4T_1(F)$, and $^4T_1(P)$ states. The absorption due to $^4A_2(F)$-$^4T_1(P)$ transition measured by us was the same as published by Wray and Allen.[18] The weak absorption due to $^4A_2(F)$-$^4T_2(F)$ transition which was not seen previously was found to be at about 3500 cm^{-1}. In the Wray and Allen spectrum of ZnSe:Co, a line at 14290 cm^{-1} is seen which can be interpreted as being due to spin-forbidden transition to the $^2T_1$ state arising from the ^2H state. From this absorption the Racah parameter C can be determined. The C parameter is not very important in our consideration because the investigated crystal-field structure of the $^4T_1(F)$ term is insensitive to the value of this parameter. The spin-orbit parameter ζ on the $^4T_1(F)$ state could be determined from an analysis of the structure of the absorption band connected with the transition to this state, as described in Sec. V B.

The calculation of energy levels of the $3d^7$ configuration has been done in a weak crystal-field scheme using $SLJM_J$ basis states.[26,27] In the $SLJM_J$ basis states, matrix elements of spin-orbit interaction[26] and crystal-field potential[27] can be expressed in terms of reduced matrix elements of unit tensor operators $V^{(11)}$ and $U^{(k)}$ given in Nielson and Koster tables[28] and 3-j and 6-j symbols tabulated by Rotenberg *et al.*[29] The well-known energies of electrostatic interaction[30] between electrons of the $3d^7$ shell for SL states are given by Racah parameters[28,31] B and C. The complete Hamiltonian, including crystal field, electrostatic, and spin-orbit interaction was built up with ap-

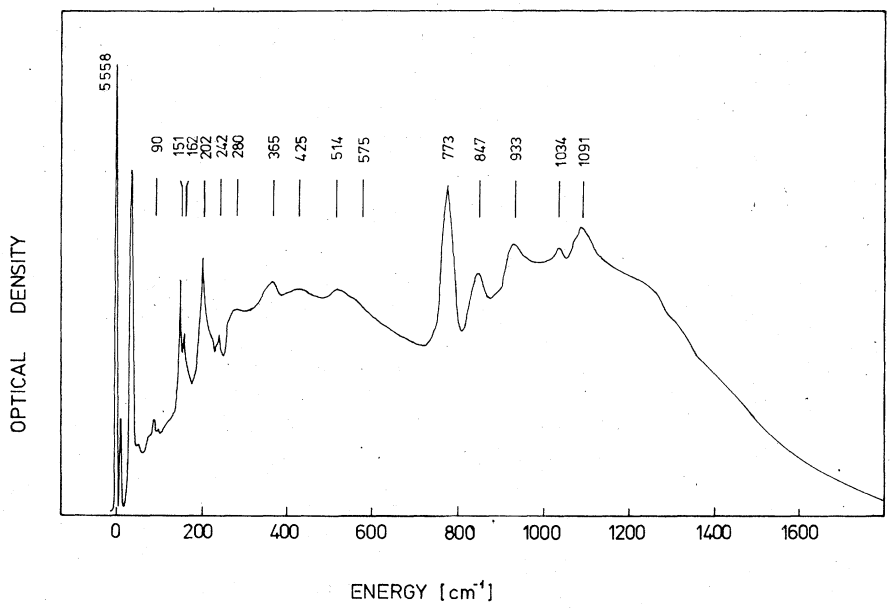

FIG. 1. $^4A_2$-$^4T_1(F)$ absorption of Co^{2+} in ZnSe at 1.5 K. Wave-number differences to the zero-phonon line (ZPL) above main lines are given.

propriate matrix elements[32] and then diagonalized to obtain the energy levels of the $3d^7$ shell. To test results for a weak-field scheme, a comparison between them and the results for a strong crystal-field coupling scheme was done. The energy levels for the $3d^7$ configuration have been independently obtained from diagonalization of the Hamiltonian built up with Runciman and Schroeder[33] and Tanabe and Sugano[34] matrices calculated in a strong-field scheme. The calculated energy levels in both schemes were exactly identical.

Next, the relative intensities of electric dipole transitions from the ground state to all excited states of the $3d^7$ configuration have been calculated. The calculation of the relative intensities has been done in "closure approximation"[27,34,35] using weak-field formulas for transition-moment matrix elements[27,35] and wave functions of $3d^7$ states derived from calculation of energy levels. The advantage of intensity calculations in the weak-field scheme is that transition-moment matrix elements are expressed in 3-j and 6-j and $U^{(k)}$ terms, similarly as in the case of energy-levels calculation.

The calculated energy levels of the $3d^7$ configuration were afterwards fitted to the centroids of the observed absorption bands. The best fit was obtained for $\Delta = 3500$ cm^{-1}, $B = 590$ cm^{-1}, $C = 1970$ cm^{-1}, and $\zeta = 385$ cm^{-1}. For these crystal-field parameters, of which spin-orbit parameter ζ is the most important, the structure of the $^4T_1(F)$ term was obtained, as shown in Fig. 4(a). The energy separation of Γ_8, Γ_7, and Γ_8' components from the lowest Γ_6 one are 321 cm^{-1}, 730 cm^{-1}, and 803 cm^{-1}, respectively. The calculated relative intensities of optical transitions to all spin-orbit components of the $^4T_1(F)$ term are also shown in Fig. 4(a). It is seen that a crystal-field theory for rigid lattice is not able to explain the complex absorption spectrum.

Next we shall consider the influence of Jahn-Teller coupling of d electrons with the lattice phonons.

IV. SYMMETRIES AND FREQUENCIES OF JAHN-TELLER ACTIVE MODES

In considering the vibronic sidebands one has to know the frequencies and symmetries of JT active modes. Relying on the facts that cobalt substitutes for zinc atoms in ZnSe and that atomic masses of cobalt and zinc are similar, it seems justified to choose the frequencies of JT active modes coincident to frequencies of phonons of the host lattice.

It seems the most likely that JT active modes will correspond to those phonons which originate from the strongest peaks of phonon density of states of the crystal. Data on the phonon density of states of ZnSe can be obtained from various optical studies[36,37] and from neutron scattering experiments.[38]

The lowest-frequency peak of phonon density of states connected with transverse-acoustic phonons[36-38] is at 70–75 cm^{-1}. This peak of phonon density of states corresponds to the TA(X) phonon. The recent optical studies[39-43] and Raman scattering data[36,44-48] give a value of TA(X) phonon frequency close to 72 cm^{-1}. The group-theoretical selection rules predict that the TA(X) phonon can create a vibrational mode of T_2 symmetry at the impurity site only.[49] However, the width of the peak of density of states of TA phonons indicates that not only phonons from X point contribute to it, but from the whole neighborhood of this point. The symmetry selection rule, valid only at the exact X point, can be broken in this case, and the vibrational mode of T_2 as well as E symmetry may originate from this peak of phonon density of states. Therefore, the calculation of vibronic levels due to JT coupling with low-frequency mode of $\hbar\omega = 72$ cm^{-1} has been done for the case of E mode and T_2 mode, as well.

The next peak of phonon density of states comes from LA branches at the energy of about 160 cm^{-1} – 170 cm^{-1}. However, this peak is very close to the much stronger peak of density of states of optical phonons, and was neglected in our considerations.

The strongest phonon density-of-states peak reported by Irvin *et al.*,[36] Kunc *et al.*,[37] and Hennion *et al.*[38] is at the frequencies 205–220 cm^{-1}. From the above papers it is known that the TO branch, flat throughout the whole Brillouin zone, contributes mostly to this density-of-states peak. Therefore, the high-frequency JT active modes can be of E as well as T_2 symmetry. For the calculation of vibronic levels due to JT coupling to high-frequency mode, the value of $\hbar\omega = 210$ cm^{-1} was used.

V. JAHN-TELLER COUPLING IN $^4T_1(F)$ TERM

A. Method

The JT-effect calculations were performed in the weak-coupling scheme first described by Ham *et al.*[5,6] and employed by Koidl *et al.*[9] and Ryskin *et al.*,[10] in the case of ZnS:Co. This scheme is based on the assumption that the JT effect is acting on the spin-orbit levels of the $^4T_1(F)$ term. The zero-order effective Hamiltonian of the $^4T_1(F)$ term is

$$\mathcal{H}_0 = \mathcal{H}_{so} + \mathcal{H}_{latt} . \quad (1)$$

The $\mathcal{H}_{so}$ is effective spin-orbit Hamiltonian for the $^4T_1(F)$ term[50]:

$$\mathcal{H}_{so} = \xi \vec{\mathcal{L}} \cdot \vec{S} + \mu(\vec{\mathcal{L}} \cdot \vec{S})^2 + \rho(\mathcal{L}_x^2 S_x^2 + \mathcal{L}_y^2 S_y^2 + \mathcal{L}_z^2 S_z^2) , \tag{2}$$

where ξ, μ, and ρ are parameters determined from the fit to the calculated spin-orbit splitting of the $^4T_1(F)$ term. The $\mathcal{H}_{latt}$ is a kinetic and an elastic energy of E- and/or T_2-mode harmonic oscillator[5,51]:

$$\mathcal{H}_{latt} = \sum_{\Gamma,\gamma} \left(\frac{1}{2m} P_{\Gamma\gamma}^2 + \tfrac{1}{2} m\omega_\Gamma^2 Q_{\Gamma\gamma}^2 \right) , \tag{3}$$

where $P_{\Gamma\gamma}$ is the γth component of the momentum conjugate to the normal coordinate $Q_{\Gamma\gamma}$, and m and ω_Γ are effective mass and frequency of the Γth normal mode ($\Gamma = \Gamma_3$ or Γ_5 for E or T_2 mode, respectively).

The energy levels due to the $\mathcal{H}_0$ Hamiltonian, because of the noninteracting $\mathcal{H}_{so}$ and $\mathcal{H}_{latt}$ parts, are given as follows:

$$E_{i N_E N_T} = E_i + N_E \hbar\omega_E + N_T \hbar\omega_T , \tag{4}$$

where E_i are energies of the Γ_6, Γ_8, Γ_7, and Γ_8' spin-orbit levels of the $^4T_1(F)$ term; N_E and N_T denote principal quantum numbers of the excited E and T_2 mode oscillator levels, respectively. These energy levels are shown in Fig. 2 for the E and T_2 mode separately.

The JT Hamiltonian, linear in normal coordinates, is introduced as perturbation to H_0,[5,51]

$$\mathcal{H}_{JT} = V_E(\mathcal{E}_\theta Q_\theta + \mathcal{E}_\epsilon Q_\epsilon) + V_T(\mathcal{T}_\xi Q_\xi + \mathcal{T}_\eta Q_\eta + \mathcal{T}_\zeta Q_\zeta) , \tag{5}$$

where V_E and V_T denote JT coupling parameters for the E and T_2 mode, respectively. These parameters are related to the appropriate JT energies

$$E_{JT}^E = V_E^2/2m\omega_E^2 \quad \text{and} \quad E_{JT}^T = 2V_T^2/3m\omega_T^2 . \tag{6}$$

The $\mathcal{E}_i$ and $\mathcal{T}_i$ in Eq. (5) are electronic operators corresponding to the $^4T_1$ state. They have been obtained from spin-orbit functions of the $^4T_1$ multiplet [33,52] and from the operators defined by Moffit and Thorson[51] for orbital triplet T_1. The $\mathcal{E}_i$ operators are given in Appendix B.

The symmetry-adapted vibronic zero-order wave functions were constructed as linear combinations of electronic functions of spin-orbit levels of the $^4T_1$ term and the symmetrized vibrational functions of the E- or T_2-mode oscillator. The E mode functions, in contrast to the method of Koidl *et al.*[9] and Maier *et al.*,[12] were obtained from the solutions of the two-dimensional oscillator in the polar coordinates: $Q_\theta = \rho\cos\varphi$ and $Q_\epsilon = \rho\sin\varphi$. These functions in T_d symmetry are simple products of angular and radial[53,54] parts:

$$\chi_{\Gamma,N,m}(\rho,\varphi) = \psi_{\Gamma,m}(\varphi) F_{N,m}(\rho) , \tag{7}$$

where Γ denotes irreducible representation A_1, A_2, or E; N is the principal quantum number of the two-dimensional oscillator; and m is the angular quantum number fulfilling the condition

$$m = N,\ N-2,\ \ldots,\ 1,\ \text{or}\ 0.$$

In T_d symmetry the angular wave functions are as follows. For $m = 0$

$$\psi_{A_1,0}(\varphi) = (2\pi)^{-1/2} . \tag{8a}$$

For $m > 0$ and for $j = 0$, $\Gamma = A_1$, or $j = 1$, $\Gamma = E_\theta$, or $j = 2$, $\Gamma = E_\theta$, where $m \equiv j \pmod 3$,

$$\psi_{\Gamma,m}(\varphi) = \pi^{-1/2}\cos m\varphi . \tag{8b}$$

Interchange of A_1 with A_2 and E_θ with E_ϵ gives

$$\psi_{\Gamma,m}(\varphi) = (-1)^{j+1}\,\pi^{-1/2}\sin m\varphi . \tag{8c}$$

This choice of vibrational wave functions extremely simplifies the E-mode calculation. The T_2-mode oscillator functions were taken as products of radial three-dimensional oscillator functions[55] and angular parts listed in tables by Altmann and Cracknell.[56]

Matrix elements of the full vibronic Hamiltonian $\mathcal{H} = \mathcal{H}_0 + \mathcal{H}_{JT}$ between vibronic wave functions were first factorized on electronic, vibrational, and recoupling matrix elements using group-theoretical formulas whose derivation is outside the scope of this paper.[57] Next, the relatively small matrices of these factors were coded in our program, and the full vibronic matrix Hamiltonian was built up automatically with these matrices on the basis of a set of vibronic quantum numbers taken as input data. The whole matrix factorized into blocks belonging to Γ_6, Γ_7, and Γ_8 representations.

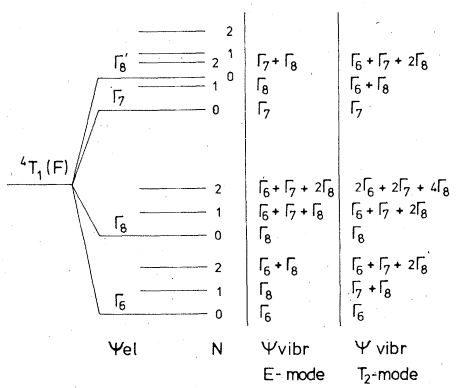

FIG. 2. Schematic drawing of the vibronic energy levels arising from coupling the $N = 0$, 1, and 2 states of an E- or T_2-mode phonon to the spin-orbit levels of the $^4T_1(F)$ term. The symmetry of vibronic states is shown.

Vibronic energy levels in the JT effect were obtained by numerical diagonalization of the matrix Hamiltonian. The relative intensities of optical transitions to vibronic levels were calculated by multiplying vibronic state zero-phonon admixture by the intensity of the corresponding zero-phonon transition for zero coupling.

The probability of error has been considerably reduced in our calculation by comparison of the results (for a small number of phonon-coupled states) with those obtained from simple unsymmetrized-wave-functions calculations.

The method adopted here for matrix diagonalization is based on the fact that all matrices in the JT effect, linear in normal coordinates, are narrow-band matrices.[58] This allowed us to apply special subroutines "bandrd" and "imtql2" described by Wilkinson and Reinsch[59] for diagonalization of the matrices which give considerable saving in time and memory space. The largest dimension of the Γ_8 matrix used in our computation for the E mode for $N=20$ of phonon-coupled states was 462×462. All computations were performed on the CDC CYBER 72 computer system in the FORTRAN extended language.

B. E-mode coupling

The calculations of vibronic energy levels of the $^4T_1(F)$ term coupled to the E-mode phonon have been done along the lines indicated in Sec. V A.

The lowest-vibronic-levels diagram for low-frequency mode of $\hbar\omega=72$ cm^{-1} is plotted in Fig. 3. The diagram has been calculated for number $N=15$ phonon-coupled states, which is sufficient to get reliable results for all presented levels.

The vibronic energy levels for $E_{JT}=0$ are spaced identically to the levels of the two-dimensional harmonic oscillator. As JT energy increases, the depression of energy of vibronic levels is observed. The vibronic levels for weak JT coupling are still equally spaced but with reduced frequency of the oscillator. The analytic expressions for the reduction of oscillator frequencies are given in Appendix A. The equation (A11) states that the decrease of the frequency of oscillator is linear with JT energy and depends on the initial spin-orbit splitting of the $^4T_1$ term. The mechanism which leads to the depression of vibronic levels is explained in Appendix B. For higher JT energies, the linear depression of vibronic levels breaks down due to interaction between states of the same symmetry, and degeneracies of upper vibronic levels are removed.

It is interesting that for E_{JT} near 445 cm^{-1} there is "crossing" of the two lowest interacting Γ_6 levels. The Γ_6 of vibronic origin for $N=2$ goes below the Γ_6 of electronic origin. That means that the electronic state coupled to $N=2$ phonons, which represents the distorted state, becomes more energetically favored than the undistorted electronic state. Therefore, the crossing of the two lowest Γ_6 levels represents transition from the dynamic to static JT effect. The cross sections through adiabatic potential energy surfaces of the $^4T_1(F)$ state for different E_{JT} are discussed in Appendix B. There it is shown that indeed for $E_{JT}>440$ cm^{-1} the lowest state is distorted into three directions of configuration coordinates space. It is also seen in Fig. 3 that in the region of E_{JT} above 450 cm^{-1} the Γ_8 level rapidly merges to the lowest Γ_6 level, and the lowest state for $E_{JT}>500$ cm^{-1} becomes orbitally triply degenerate. This is what one can expect for the static JT effect due to E mode.

The characteristic feature of JT effect is also a transfer of intensities of optical transition from electronic components of the $^4T_1(F)$ term to vibronic sidebands. The calculated energies and intensities for all vibronic states of the $^4T_1(F)$ term for three JT energies are shown in Fig. 4. Some general conclusions can be drawn from these results:

(i) The intensity to the Γ_6 spin-orbit component is transferred to upper states of Γ_6 symmetry of vibronic origin for $E_{JT}>0$. The transfer of intensity

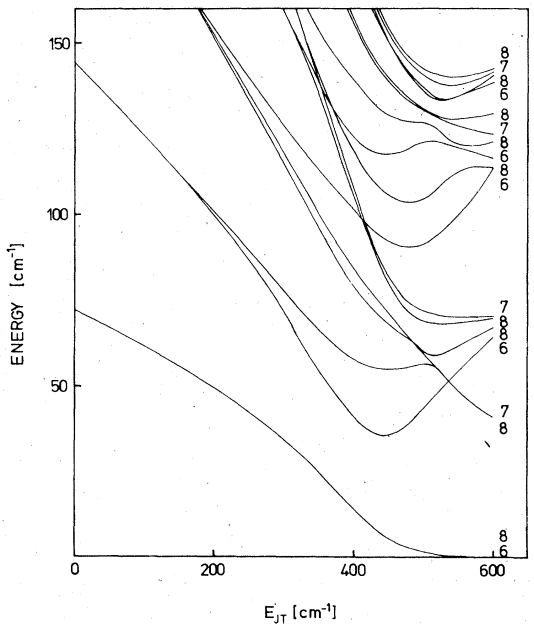

FIG. 3. Lowest vibronic levels of the $^4T_1$ term for E mode of $\hbar\omega=72$ cm^{-1} as a function of JT energy (E_{JT}), calculated for $N=15$ of phonon-coupled states. The energies of vibronic levels are given with respect to the lowest Γ_6 electronic state. The numbers on the right-hand side are abbreviations for Γ_6, Γ_7, and Γ_8.

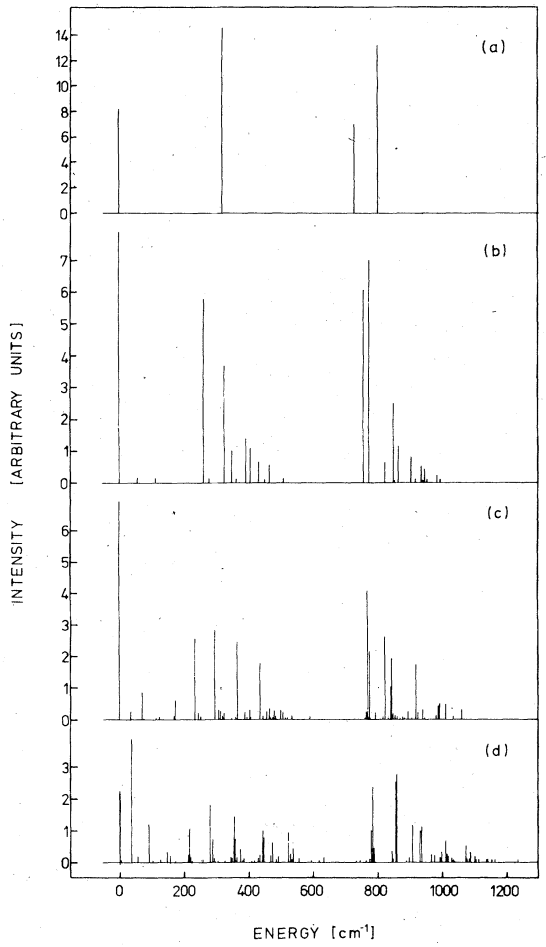

FIG. 4. (a) Energy positions and intensities of the spin-orbit components of the $^4T_1(F)$ term, calculated from rigid-lattice crystal-field theory. (b)–(d) The effect of E-mode coupling of acoustical phonon ($\hbar\omega = 72$ cm^{-1}), calculated for $N = 15$ of phonon-coupled states for (b) $E_{JT} = 150$ cm^{-1}, (c) $E_{JT} = 300$ cm^{-1}, (d) $E_{JT} = 450$ cm^{-1}.

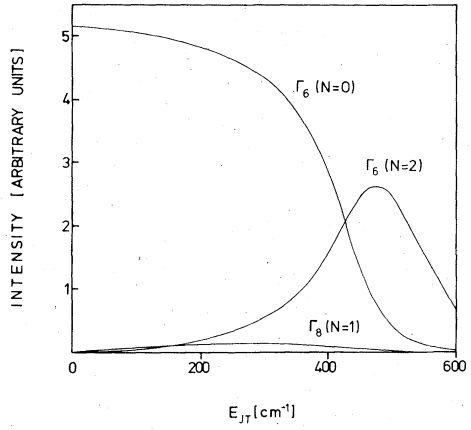

FIG. 5. Intensities of optical transitions to the lowest Γ_6, Γ_8, and Γ_6 vibronic states of the $^4T_1$ term as a function of JT energy for coupling to low-frequency E mode ($\hbar\omega = 72$ cm^{-1}).

from Γ_6 zero-phonon line (ZPL) to the Γ_6 of vibronic origin for $N = 2$ as a function of E_{JT} is shown in Fig. 5. The inversion of intensities between the two Γ_6 takes place in the region of E_{JT} where these levels cross.

(ii) The Γ_7 and Γ_8' spin-orbit components at 730 and 803 cm^{-1} are not essentially affected by the presence of JT coupling. They are not depressed relative to ZPL, and are even slightly shifted to higher energies. This fact is also discussed in Appendix B. The transfer of intensities from electronic Γ_7 and Γ_8' components takes place only to upper-lying vibronic sidebands. Optical transitions to the electronic Γ_7 and Γ_8' states play the role of zero-phonon lines of the other part of the absorption band. The energy position of these lines is mainly determined by the value of spin-orbit parameter ζ. On the basis of the above conclusion, the value of the spin-orbit parameter has been obtained.

(iii) The spin-orbit Γ_8 state at 321 cm^{-1} is depressed with increase of E_{JT}. The Γ_8 electronic state interacts strongly and loses its intensity to several upper and lower Γ_8 states of vibronic origins. As a result the broadband centered at 320 cm^{-1} is created.

The diagram of lowest vibronic levels for JT coupling with optical mode of $\hbar\omega = 210$ cm^{-1} is shown in Fig. 6. As in the case of low-frequency mode, the lowest vibronic states are depressed. The spin-orbit component Γ_8 is also depressed, reminiscent of the situation described by the Ham effect.

C. Comparison with experiment

In Sec. V B we discussed the main mechanisms of creation of vibronic sidebands. It was shown that the effect of depression of vibronic levels is responsible for the structures nearest to ZPL.

Therefore, one of the main tests of the comparison of calculated lines with the experimental spectrum is the energy position and intensities of the lines nearest to ZPL. The other such test is the overall shape of the whole calculated absorption band which in the experiment consists of two parts.

The ZPL and its sidebands centered at energies 10.5, 35, and 53 cm^{-1} are shown in Fig. 7. The best fit of calculated positions and intensities of these lines for E mode of $\hbar\omega = 72$ cm^{-1} and $E_{JT} = 425$ cm^{-1} is shown also in Fig. 7. The positions of the calculated Γ_6, Γ_8, and Γ_6 lines agree with experimental ones with an accuracy of 2 cm^{-1}. The

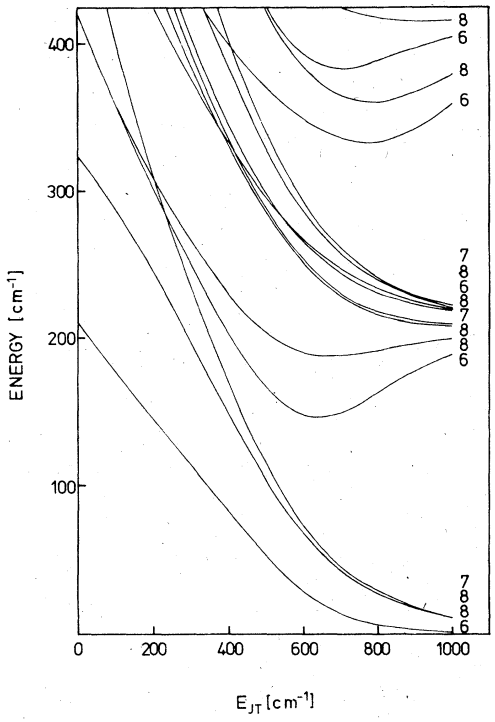

FIG. 6. Lowest vibronic levels of the $^4T_1$ term for E mode of $\hbar\omega = 210$ cm^{-1} as a function of JT energy, calculated for $N = 15$ of phonon-coupled states. The energies of vibronic levels are given with respect to the lowest Γ_6 electronic state. The numbers are abbreviations for Γ_6, Γ_7 and Γ_8.

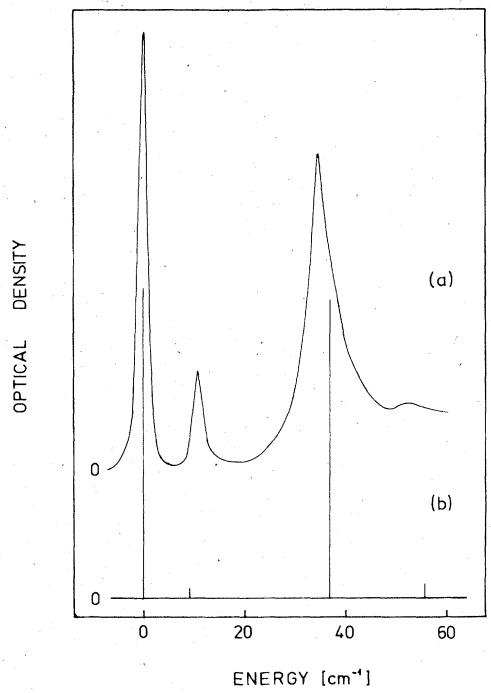

FIG. 7. Comparison of the lowest-energy experimental lines of the $^4T_1(F)$ absorption band with theoretical predictions. (a) Optical density at 1.5 K vs wave-number differences to the ZPL. (b) Positions and intensities of the lines calculated for E mode of $\hbar\omega = 72$ cm^{-1} and for $E_{JT} = 425$ cm^{-1}.

shoulder at 53 cm^{-1} is also explained as being due to the presence of the Γ_8 state. The intensity of the line 10 cm^{-1} is predicted to be much weaker than the intensity of ZPL and 35 cm^{-1} line. The calculation also predicts almost equal intensity of the 35 cm^{-1} line and ZPL, which reasonably agrees with experiment, although the integrated absorptions indicate that the 35 cm^{-1} line is more intense. It is worth mentioning that efforts to get similar fit for E mode of $\hbar\omega = 50$ cm^{-1}, which corresponds to the energy of the TA(L) phonon, were not successful. The fit obtained in this case was much worse than the one for $\hbar\omega = 72$ cm^{-1}.

In the case of coupling to E-mode optical phonon of $\hbar\omega = 210$ cm^{-1}, the calculated positions of the first lines agree reasonably with experimental ones for $E_{JT} = 750$ cm^{-1}. But in this case the sequence of the lowest states is Γ_6, Γ_8, and Γ_8, with intensity of Γ_6 always strongest, which is in disagreement with experiment. Also, the calculated positions and intensities of all other lines are in disagreement with the experimental spectrum as can be seen in Fig. 8. The coupling to E-mode optical phonon alone as being predominant was rejected also, on the basis of moment analysis appearing in Sec. VI.

The calculated positions and intensities of all vibronic levels for $\hbar\omega = 72$ cm^{-1} and $E_{JT} = 425$ cm^{-1} are compared with the experimental spectrum in Fig. 9. The calculation has been made for number $N = 20$ of phonon-coupled states, and, within a few cm^{-1}, it is an exact solution for all vibronic levels. The agreement with the experimental spectrum is quite good. The characteristic double-band absorption is reflected in the calculation. In addition almost all absorption lines are reproduced in the calculation with good accuracy. The calculation predicts a decrease of the energy of the lowest Γ_6 ZPL of 66 cm^{-1}. This value is considerably smaller than $E_{JT} = 425$ cm^{-1}, showing the stabilizing influence of spin-orbit coupling against JT distortion.

D. Number of phonon-coupled states

The results of calculations presented in the previous sections are very sensitive to the number of phonon-coupled states included in the calculations. The convergence of the calculations in general

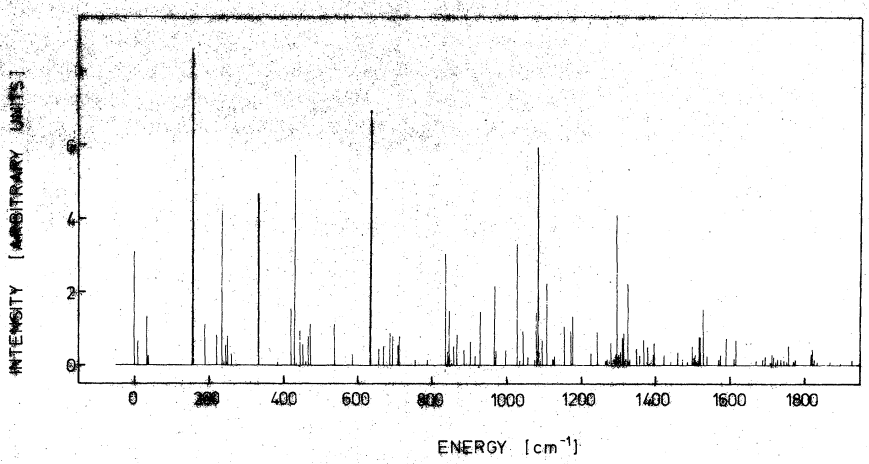

FIG. 8. Positions and intensities of the calculated lines for coupling of the ${}^4T_1(F)$ term to the E-mode optical phonon ($\hbar\omega = 210$ cm^{-1}) for $E_{JT} = 750$ cm^{-1}. The calculations have been done for $N = 15$ of phonon-coupled states.

was very slow. The convergence depends very much on the the magnitude of Jahn-Teller effect, on the energy of the phonon, and also depends on the origin of vibronic level.

The influence of the number of phonon-coupled states on the positions of the lowest Γ_8 and Γ_6 levels is shown in Fig. 10. The results for $N = 15$ are the same as for greater N and therefore this number of phonon-coupled states produce an exact solution for the lowest levels up to $E_{JT} = 600$ cm^{-1}. It is seen that it is possible to get such an exact solution for $E_{JT} < 200$ cm^{-1} for even $N = 4$. But this refers only to the lowest levels. The convergence for higher vibronic levels is even slower than those presented in Fig. 10.

It seems that Koidl *et al.*'s[9] estimation that number $N = 4$ of phonon-coupled states is sufficient

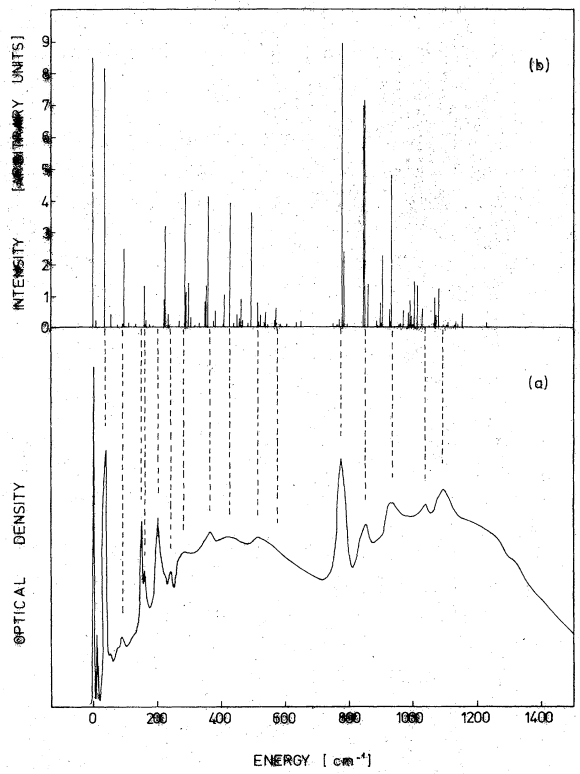

FIG. 9. Comparison of the ${}^4T_1(F)$ absorption spectrum with theoretical calculations. (a) Optical density of the whole band at 1.5 K. (b) Positions and intensities of the lines calculated for coupling to E mode of $\hbar\omega = 72$ cm^{-1} and for $E_{JT} = 425$ cm^{-1}. The calculation has been done for $N = 20$ of phonon-coupled states.

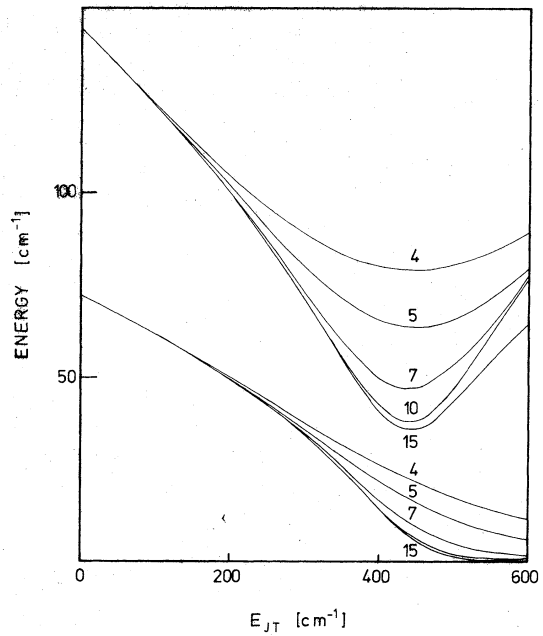

FIG. 10. Positions of the lowest vibronic levels of the ${}^4T_1$ term due to E mode of $\hbar\omega = 72$ cm^{-1} as a function of JT energy, calculated for different numbers of phonon-coupled states (these numbers are given above the lines). The energies of the levels are given with respect to the Γ_6 electronic state.

to get reliable results is over optimistic. The Koidl *et al.*'s calculations for the $^4T_1(F)$ term in ZnS:Co have been done for $E_{JT} = 350$ cm^{-1}, where for the lowest states one can get for $N = 4$ reliable results which correspond to the results for $N = \infty$, but for smaller JT energies. But the results for upper vibronic states cannot be accurate. Also their calculations for two E phonons can be, at most, qualitative.

To get reliable results for $E_{JT} = 425$ cm^{-1} for all vibronic levels it is necessary to carry out calculations up to $N = 20$ of phonon-coupled states. The most sensitive levels for number of phonons are between 150 and 500 cm^{-1}, which originates from the Γ_8 electronic state. On the other hand, the levels above 800 cm^{-1} do not depend so strongly on the number of phonon-coupled states. The positions and intensities of vibronic levels at about 800–1000 cm^{-1} were quite well established for $N = 15$. This can be understood on the basis of cross sections through the adiabatic potential energy surfaces discussed in Appendix B. The energy surfaces connected with Γ_7 and Γ_8' states at 730 and 803 cm^{-1} are not essentially affected by JT coupling, in contrast to the surfaces connected with the Γ_8 state at 321 cm^{-1}.

E. T_2 mode coupling

As was shown in Sec. V C, the observed spectrum can be very well explained by predominant JT coupling to the low-frequency E mode. But that does not exclude the possibility of obtaining equally good fit for coupling to the T_2 mode, as well.

The vibronic energy diagram of the $^4T_1(F)$ term coupled to the T_2 mode is shown in Fig. 11. The diagram has been done for $\hbar\omega = 72$ cm^{-1} and for the same value of spin-orbit parameter ζ as in the case of the E mode. Due to the extreme complexity of T_2 mode, the numerical calculation has been carried out to $N = 5$ phonon-coupled states only. In spite of the relatively small number of phonon-coupled states included in T_2-mode calculation, the diagrams for the T_2 mode and E mode shown in Figs. 11 and 3, respectively, are similar in some respects.

For small E_{JT}, the depression of vibronic levels is the same for both modes. This can be understood on the basis of the expression for the depression of the energy of vibronic states given in Appendix A. The expressions for reduction of E-mode and T_2-mode frequency, obtained from Eq. (A11) and Table I, are as follows:

$$\omega_E' = \omega_E \left[1 - E_{JT}^E \left(\frac{1}{10}\,\frac{E_8}{E_8^2 - (\hbar\omega)^2} + \frac{9}{10}\,\frac{E_{8'}}{E_{8'}^2 - (\hbar\omega)^2}\right)\right], \tag{9}$$

$$\omega_T' = \omega_T \left[1 - E_{JT}^T \left(\frac{1}{10}\,\frac{E_8}{E_8^2 - (\hbar\omega)^2} + \frac{4}{10}\,\frac{E_{8'}}{E_{8'}^2 - (\hbar\omega)^2} + \frac{5}{10}\,\frac{E_7}{E_7^2 - (\hbar\omega)^2}\right)\right], \tag{10}$$

where E_8, E_7, and $E_{8'}$ are energies of Γ_8, Γ_7, and Γ_8' electronic states relative to the Γ_6 state of the $^4T_1(F)$ term.

Taking the values of E_8, E_7, and $E_{8'}$ as given in Sec. III, and $\hbar\omega = 72$ cm^{-1}, one obtains

$$\omega_E' = \omega_E(1 - 1.458 \times 10^{-3} E_{JT}^E)\,, \tag{11}$$

$$\omega_T' = \omega_T(1 - 1.522 \times 10^{-3} E_{JT}^T)\,, \tag{12}$$

where E_{JT} is in cm^{-1}.

The reductions of E-mode and T_2-mode frequencies are almost the same because for the $^4T_1(F)$ term $E_{8'} \cong E_7$ (in the first order of perturbation calculation in crystal-field theory $E_{8'} = E_7$).

The depression of vibronic levels leads finally to the "crossing" of the two lowest Γ_6 levels which takes place at almost the same E_{JT} for both the E and T_2 modes. But the energy distance between two interacting Γ_6 levels for the T_2 mode is such that it is impossible to get reasonable fit to experimental lines. It is clear, however, that $N = 5$ phonon-coupled states are not enough to get reliable results for the lowest vibronic levels (Sec. V D). The comparison between Figs. 10 and 11 in-

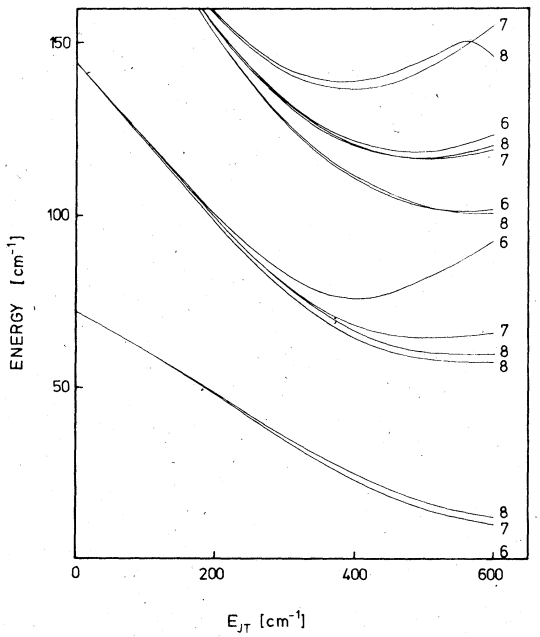

FIG. 11. Lowest vibronic levels of the $^4T_1$ term for coupling to T_2-mode of $\hbar\omega = 72$ cm^{-1} as a function of JT energy, calculated for $N = 5$ of phonon-coupled states. The energies of vibronic levels are given with respect to the Γ_6 electronic state. The numbers on the right-hand side are abbreviations for Γ_6, Γ_7, and Γ_8.

dicates that the results for T_2 mode for $N=5$ correspond to the ones for E mode for $N=4$. It seems that convergence for the T_2 mode is even slower than for the E mode. Therefore, the calculated positions of the Γ_8, Γ_7, and Γ_6 states shown in Fig. 11 will be in reality pushed down to lower energies. The decrease of Γ_6 can be quite strong similar to the one shown in Fig. 10. Similarly, as in the case of the E mode, the strong transfer of intensity from ZPL Γ_6 to the vibronic Γ_6 state takes place for E_{JT} close to the "crossing" of these two levels. The intensity of the lowest Γ_8 and Γ_7 levels is weak and, because they lie very close together, it is possible that they were not resolved in the experiment. Therefore, it is possible that equally good fit as was obtained for the E mode can be also obtained for the T_2 mode, as far as the lowest levels are concerned.

The question arises if equally good fit can be obtained for the shape of the whole absorption band for the T_2-mode coupling. The calculated positions and intensities for all vibronic levels for $\hbar\omega = 72$ cm^{-1} and $E_{JT} = 400$ cm^{-1} are shown in Fig. 12. In spite of the fact that the results are not accurate due to insufficient number of phonon-coupled states, they qualitatively reproduce the double-band shape of the absorption.

Therefore, the possibility that JT coupling with a low-frequency mode of T_2 symmetry is responsible for the observed absorption spectrum cannot be ruled out.

The high-frequency optical mode of T_2 symmetry, similar to the case of E symmetry, was not successful in explaining the experimental spectrum. It was not possible to get reasonable fit

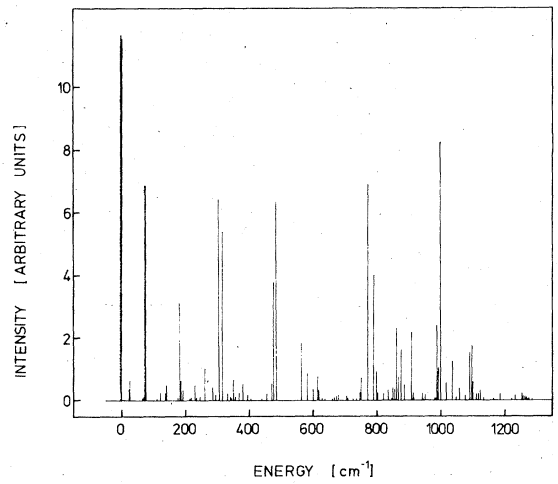

FIG. 12. Energy positions and intensities of the calculated lines for coupling of the $^4T_1(F)$ term to T_2 mode of $\hbar\omega = 72$ cm^{-1} and for $E_{JT} = 400$ cm^{-1}. The calculation has been done for $N=5$ of phonon-coupled states.

for the lines nearest to ZPL and to get the characteristic double-band shape of experimental absorption. The coupling to the T_2 mode optical phonon alone as being predominant was rejected also, for reasons included in the discussion of moment analysis below.

VI. DISCUSSION

It was shown in Sec. V E that the symmetry of the JT active mode cannot be determined from absorption measurements alone. However, the recent optical experiments done under uniaxial pressure for ZnS:Co indicate that the line next to ZPL is of Γ_8 symmetry.[60] That indicates that the low-frequency JT active mode is of E symmetry. Therefore, relying on the analogy between spectra of ZnS:Co and ZnSe:Co, it seems that in our case the coupling to E mode is also more likely.

The presented fit of calculated absorption to the observed spectrum was done for two adjustable parameters E_{JT} and ζ. The frequency of the JT active mode was fixed to the frequency of the peak of density of states of transverse acoustic phonons. The spin-orbit parameter was adjusted to the separation of the two parts of the absorption band. The JT energy was chosen to give appropriate energy positions and intensities of the first absorption lines. Considering this, the obtained fit to the experimental spectrum is very good, indeed.

On the other hand, there are high-energy tails of the two parts of the absorption spectrum which are not reflected in the calculations. That implies that, beside the JT coupling to low-frequency mode, there is also appreciable coupling to high-frequency totally symmetric and JT active modes.

The first and second moment[61] of the absorption line shape were evaluated in order to estimate the contribution from the other phonons. The first moment, which is the energy separation of the centroid of the absorption band from ZPL, is 800 cm^{-1}. The experimentally determined second moment is equal to 1.81×10^5 cm^{-2}. The values of the first and second moment cannot be explained by coupling to high-frequency JT active mode alone. For E-mode coupling of $\hbar\omega = 210$ cm^{-1} and $E_{JT} = 750$ cm^{-1}, the calculated first and second moment yield 783 cm^{-1} and 2.53×10^5 cm^{-2}, respectively, the latter being about 40% higher than the experimental one. For the T_2-mode coupling of the same frequency, an even higher value for the second moment is obtained. This is an additional argument for ruling out the possibility of predominant coupling to the high-frequency modes.

The predominant coupling to low-frequency mode partly explains the values of both modes. The

sum of spin-orbit and JT contribution to the first and second moment for $\hbar\omega = 72$ cm^{-1} and $E_{JT} = 425$ cm^{-1} is 525 cm^{-1} and 1.26×10^5 cm^{-2}, respectively. Therefore, the stabilization energy 275 cm^{-1} and value of 0.55×10^5 cm^{-2} of the second moment should be accounted as being due to all totally symmetric A_1 and high-frequency JT active modes.

The unexplained parts of both moments are given by

$$\langle E \rangle = \sum E^A_{\text{stab}} + \sum{}' E^E_{\text{stab}} + \sum E^T_{\text{stab}}, \tag{13}$$

$$\langle E^2 \rangle = \sum E^A_{JT}\hbar\omega_A + \sum{}' E^E_{JT}\hbar\omega_E + \sum E^T_{JT}\hbar\omega_T. \tag{14}$$

The primes in the sums over E modes indicate that the acoustical phonon $\hbar\omega = 72$ cm^{-1} has been removed from the sums. The following formulas apply for stabilization energies appearing in Eq. (13).

$$E^A_{\text{stab}} = E^A_{JT}, \tag{15}$$

and, from Appendix A, Eq. (A10) (for small E_{JT}),

$$E^E_{\text{stab}} = B^E E^E_{JT}, \tag{16}$$

$$E^T_{\text{stab}} B^T E^T_{JT}, \tag{17}$$

where

$$B^E = \hbar\omega_E\left[\tfrac{1}{10}(E_8 + \hbar\omega_E)^{-1} + \tfrac{9}{10}(E_{8'} + \hbar\omega_E)^{-1}\right], \tag{18}$$

$$B^T = \tfrac{3}{2}\hbar\omega_T\left[\tfrac{1}{10}(E_8 + \hbar\omega_T)^{-1} + \tfrac{4}{10}(E_{8'} + \hbar\omega_T)^{-1} + \tfrac{5}{10}(E_7 + \hbar\omega_T)^{-1}\right]. \tag{19}$$

We shall assume that the main contribution to $\langle E \rangle$ and $\langle E^2 \rangle$ is due to coupling with one high-frequency E (or T_2) mode and various totally symmetric A_1 modes. To simplify the problem of coupling with various totally symmetric modes, it is convenient to introduce the average frequency $\langle \hbar\omega_A \rangle$ of all A_1 phonons. In this approximation

$$\sum E^A_{JT}\hbar\omega_A = E_A\langle \hbar\omega_A \rangle, \tag{20}$$

where

$$E_A = \sum E^A_{JT}. \tag{21}$$

It seems reasonable that the average frequency of all A_1 phonons should be about 150–170 cm^{-1}. Considering these, Eqs. (13) and (14) simplify to a form

$$\langle E \rangle = E_A + B^E E^E_{JT}, \tag{22}$$

$$\langle E^2 \rangle = E_A\langle \hbar\omega_A \rangle + E^E_{JT}\hbar\omega_E, \tag{23}$$

and for $\hbar\omega_E = 210$ cm^{-1} one obtains E^E_{JT} from 78 to 48 cm^{-1} and E_A from 257 to 264 cm^{-1}, respectively. For optical T_2-mode coupling, there is interchange of subscript E into T in above equations, and one obtains E^T_{JT} from 87 to 55 cm^{-1} and E_A from 244 to 256 cm^{-1}, respectively. From the above estimation it is seen that the coupling to totally symmetric modes is mainly responsible for the high-energy tails in the absorption spectrum. The JT coupling to the high-frequency optical mode is relatively weak.

The interesting problem of the dominant role of JT effect due to low-frequency acoustical mode ($E^E_{JT}/\hbar\omega_E = 5.9$) over high-frequency optical-mode contribution arises ($E^E_{JT}/\hbar\omega_E \cong 0.3$, or even less when there is simultaneous coupling to the E and T_2 optical modes). The values of JT coupling coefficients for the E modes V_E defined in Eq. (6), answer this question. Taking for mass corresponding to E mode, the mass of the Se atom, and $E^E_{JT} = 425$ cm^{-1}, and $\hbar\omega = 72$ cm^{-1}, the value of $V_E = 0.40$ eV/Å is obtained. The estimation of E^E_{JT} for high-frequency optical mode gives the value of V_E at most from 0.39 to 0.50 eV/Å. The coefficient V_E is roughly the same for JT coupling for low-frequency as for high-frequency modes. The smaller E_{JT} connected with the optical mode is a consequence of the higher frequency of this mode according to the relation $E_{JT} \sim \omega^{-2}$. The constancy of V_E for coupling to all phonons implies that JT energy should be the highest for coupling to low-frequency phonons.

VII. CONCLUSIONS

A complete comparison between experimental results and the predictions of JT model has been presented. It is shown that for the $^4T_1(F)$ state the JT coupling is predominantly with a low-frequency mode originating from the peak of density of states of transverse-acoustic phonons of ZnSe. The effect of depression of this JT active mode frequency is observed and explained.

The symmetry of this JT active mode is most likely of E character. The distinction between E and T_2 symmetry of the mode on the basis of absorption data alone is not simple. This is partly because the depression of phonon frequency is almost the same in the case of E- and T_2-mode coupling as analytic expressions derived in this work and numerical calculations demonstrate.

The numerical calculation also shows how the transition from the dynamic to static JT effect occurs as a result of depression of vibronic levels.

The $^4T_1(F)$ state of Co^{2+} in ZnSe suffers dynamic JT effect close to the point where transition to static distortion takes place.

ACKNOWLEDGMENT

We are grateful to J. W. Allen of Wolfson Institute of Luminescence at St. Andrews University,

Scotland, for supplying us with crystals of ZnSe:Co.

APPENDIX A: JT DEPRESSION OF VIBRONIC LEVELS: PERTURBATION TREATMENT OF THE $^4T_1(F)$ STATE COUPLED TO E AND T_2 MODE

The weak-coupling scheme of the JT effect allows derivation of analytic expressions for the depression of vibronic levels. This method was applied for the first time by Ham *et al.* to the case of the $^5T_2$ state[5,6] of Fe(d^6) and to the case of s and p states in F centers.[62] We shall adapt a similar approach to the case of the $^4T_1(F)$ state.

Let us consider the Γ_6 electronic state of the $^4T_1(F)$ term, described by ket $|\Gamma\gamma\rangle$ (where γ is the $+\frac{1}{2}$ or $-\frac{1}{2}$ component of Γ_6), which interacts with the group of remaining electronic states $|\Gamma'\gamma'\rangle$ of the same term (where Γ' may be Γ_7, Γ_8, and Γ_8' and γ' is component of Γ'). We shall consider JT interaction due to E and/or T_2 mode within the whole term. Each electronic state $|\Gamma\gamma\rangle$ will be connected with the ladder of levels of a p-dimensional harmonic oscillator (where $p=2$ for E mode and $p=3$ for T_2 mode). The vibronic wave functions will be described by kets $|\Gamma\gamma\bar{n}\rangle$ where $\bar{n}$ is a set of simple quantum numbers $n_1,\ldots,n_p$ of this harmonic oscillator. We shall calculate the change in energy of vibronic states in the first and second order of perturbation theory. The linear JT Hamiltonian due to $\bar{\Gamma}$ mode will be considered as the perturbation. It can be rewritten as follows:

$$\mathcal{H}_{JT} = V_{\bar{\Gamma}} \sum_{\bar{\gamma}} \mathcal{S}_{\bar{\gamma}}(\bar{\Gamma}) Q_{\bar{\gamma}}(\bar{\Gamma}) , \tag{A1}$$

where $\bar{\Gamma}$ denotes the irreducible representation of the mode ($\bar{\Gamma}=\Gamma_3$ for E mode and $\bar{\Gamma}=\Gamma_5$ for T_2 mode) and $\bar{\gamma}$ is a component of $\bar{\Gamma}$.

It is well known that the Kramers doublet Γ_6 does not suffer JT effect in the first order. However, in the second order, the vibronic levels $|\Gamma\gamma\bar{n}\rangle$ (where $\Gamma=\Gamma_6$) are influenced by JT interaction with $|\Gamma'\gamma'\bar{n}'\rangle$ vibronic levels (where $\Gamma'=\Gamma_8,\Gamma_8'$ for E mode and $\Gamma'=\Gamma_7,\Gamma_8,\Gamma_8'$ for T_2 mode). The change ΔE in the energy of $|\Gamma\gamma\bar{n}\rangle$ vibronic state is then as follows:

$$\Delta E = \sum_{\Gamma'\gamma'\bar{n}'} \frac{\langle\Gamma\gamma\bar{n}|\mathcal{H}_{JT}|\Gamma'\gamma'\bar{n}'\rangle\langle\Gamma\gamma\bar{n}|\mathcal{H}_{JT}|\Gamma'\gamma'\bar{n}'\rangle^*}{E+N\hbar\omega_{\bar{\Gamma}}-E'-N'\hbar\omega_{\bar{\Gamma}}} , \tag{A2}$$

where E and E' are energies of electronic states Γ and Γ', $N=\sum_{i=1}^{p} n_i$ and $N'=\sum_{i=1}^{p} n_i'$ are principal quantum numbers of the $\bar{\Gamma}$-mode p-dimensional oscillator, and $\omega_{\bar{\Gamma}}$ is its frequency.

The matrix element in Eq. (A2) of $\mathcal{H}_{JT}$ given in Eq. (A1) separates on electronic and vibrational parts

$$\langle\Gamma\gamma\bar{n}|\mathcal{H}_{JT}|\Gamma'\gamma'\bar{n}'\rangle = V_{\bar{\Gamma}} \sum_{\bar{\gamma}} \langle\Gamma\gamma|\mathcal{S}_{\bar{\gamma}}(\bar{\Gamma})|\Gamma'\gamma'\rangle\langle\bar{n}|Q_{\bar{\gamma}}(\bar{\Gamma})|\bar{n}'\rangle . \tag{A3}$$

It follows from the Wigner-Eckart theorem[34,52] that

$$\langle\Gamma\gamma|\mathcal{S}_{\bar{\gamma}}(\bar{\Gamma})|\Gamma'\gamma'\rangle = (\Gamma)^{-1/2}\langle\Gamma\|\mathcal{S}(\bar{\Gamma})\|\Gamma'\rangle\langle\Gamma\gamma|\bar{\Gamma}\bar{\gamma}\Gamma'\gamma'\rangle , \tag{A4}$$

where (Γ) denotes the dimension of Γ representation, $\langle\Gamma\|\mathcal{S}(\bar{\Gamma})\|\Gamma'\rangle$ is the so-called reduced matrix element, and $\langle\Gamma\gamma|\bar{\Gamma}\bar{\gamma}\Gamma'\gamma'\rangle$ are Clebsch-Gordan coefficients tabulated for all point groups by Koster *et al.*[52]

Considering above, one obtains

$$\begin{aligned}\sum_{\gamma'} \langle\Gamma\gamma\bar{n}|\mathcal{H}_{JT}|\Gamma'\gamma'\bar{n}'\rangle\langle\Gamma\gamma\bar{n}|\mathcal{H}_{JT}|\Gamma'\gamma'\bar{n}''\rangle^* &= |V_{\bar{\Gamma}}|^2(\Gamma)^{-1}|\langle\Gamma\|\mathcal{S}(\bar{\Gamma})\|\Gamma'\rangle|^2 \\ &\times \sum_{\bar{\gamma}\bar{\gamma}'} \langle\bar{n}|Q_{\bar{\gamma}}(\bar{\Gamma})|\bar{n}'\rangle\langle\bar{n}|Q_{\bar{\gamma}'}(\bar{\Gamma})|\bar{n}''\rangle \\ &\times \sum_{\gamma'} \langle\Gamma\gamma|\bar{\Gamma}\bar{\gamma}\Gamma'\gamma'\rangle^*\langle\Gamma\gamma|\bar{\Gamma}\bar{\gamma}'\Gamma'\gamma'\rangle . \end{aligned} \tag{A5}$$

As an inspection of tables of Clebsch-Gordan coefficients shows the following "orthogonality" relation holds for $\Gamma=\Gamma_6$, $\bar{\Gamma}=\Gamma_3$, Γ_5, and Γ' appearing in the product of $\bar{\Gamma}\times\Gamma$:

$$\mathrm{Re}\sum_{\gamma'} \langle\Gamma\gamma|\bar{\Gamma}\bar{\gamma}\Gamma'\gamma'\rangle^*\langle\Gamma\gamma|\bar{\Gamma}\bar{\gamma}'\Gamma'\gamma'\rangle = (\bar{\Gamma})^{-1}\delta(\bar{\gamma},\bar{\gamma}') . \tag{A6}$$

It may be also shown from the orthogonality of the oscillator wave functions and from the well-known formula for one-dimensional harmonic oscillator

$$\langle n|Q|n'\rangle = \alpha[n^{1/2}\delta_{n',n-1} + (n+1)^{1/2}\delta_{n',n+1}] , \tag{A7}$$

where

$$\alpha = (\hbar/2m\omega_{\bar{\Gamma}})^{1/2} ,$$

that

$$\sum_{\bar{\gamma}\bar{n}'} \frac{|\langle\bar{n}|Q_{\bar{\gamma}}(\bar{\Gamma})|\bar{n}'\rangle|^2}{E-E'+\hbar\omega_{\bar{\Gamma}}(N-N')} = \alpha^2\left(\frac{N+p}{E-E'-\hbar\omega_{\bar{\Gamma}}}+\frac{N}{E-E'+\hbar\omega_{\bar{\Gamma}}}\right) . \tag{A8}$$

From Eqs. (A1)–(A8) one finally obtains the formula

$$\Delta E = \alpha^2|V_{\bar{\Gamma}}|^2 \sum_{\Gamma'} (\Gamma)^{-1}(\bar{\Gamma})^{-1}|\langle\Gamma\|\mathcal{S}(\bar{\Gamma})\|\Gamma'\rangle|^2 [(N+p)/(E-E'-\hbar\omega_{\bar{\Gamma}})+N/(E-E'+\hbar\omega_{\bar{\Gamma}})] . \tag{A9}$$

The change in energy ΔE does not depend on γ, and thus is the same for all component states γ of vibronic levels. Therefore, in second order of perturbation theory, highly degenerated vibronic levels connected to the Γ_6 electronic state remain unsplit, and are described by the principal oscillator quantum number N. The absolute value of the energy change of the ground-state oscillator level ($N=0$), being stabilization energy, is equal to

$$E_{\text{stab}} = p\alpha^2 \left| V_{\bar{\Gamma}} \right|^2 \sum_{\Gamma'} (\Gamma)^{-1}(\bar{\Gamma})^{-1} \left| \langle \Gamma \| \mathcal{E}(\bar{\Gamma}) \| \Gamma' \rangle \right|^2 (E' - E + \hbar\omega_{\bar{\Gamma}})^{-1} . \tag{A10}$$

The energy of the Nth level relative to the ground level is therefore proportional to N. This enables us to formulate the theorem that vibronic energy levels connected to electronic state Γ_6, interacting in the second-order of the perturbation theory with other electronic levels via Jahn-Teller active modes of E or T_2 symmetry, are the same as vibrational levels of the harmonic oscillator with reduced frequency $\omega'_{\bar{\Gamma}}$. The expression for reduced frequency $\omega'_{\bar{\Gamma}}$ is as follows:

$$\omega'_{\bar{\Gamma}} = \omega_{\bar{\Gamma}} \left[1 + C_{\bar{\Gamma}} \sum_{\Gamma'} \frac{2(\Gamma)^{-1}(\bar{\Gamma})^{-1} \left| \langle \Gamma \| \mathcal{E}(\bar{\Gamma}) \| \Gamma' \rangle \right|^2 (E - E')}{(E - E')^2 - (\hbar\omega_{\bar{\Gamma}})^2} \right] , \tag{A11}$$

where

$C_{\bar{\Gamma}} = E^E_{\text{JT}}$ for E mode,

$C_{\bar{\Gamma}} = \frac{3}{4} E^T_{\text{JT}}$ for T_2 mode.

The reduced matrix elements appearing above can be calculated applying the Wigner-Eckart theorem, Eq. (A4), to the nonzero matrix elements of electronic operators $\mathcal{E}_{\bar{\gamma}}(\bar{\Gamma})$ which are defined in Sec. V A. The reduced matrix elements are listed in Table I.

This theorem may be easily extended to the case of various simultaneously interacting modes because it appears that the second-order reductions of frequencies may be treated separately for each mode.

The above results are valid under the assumption of application of perturbation theory, i.e., as long as the following conditions are satisfied:

$$\hbar\omega < \left| E - E' \right| \quad \text{and} \quad E_{\text{JT}} \lesssim \left| E - E' \right| ,$$

as in the case of weak JT effect.

The above results apply to a more general case of ${}^{2S+1}T_i$ terms (where $S = \frac{1}{2}$ or $\frac{3}{2}$ and $i = 1, 2$). The reduced matrix elements $\langle \Gamma \| \mathcal{E}(\bar{\Gamma}) \| \Gamma' \rangle$ for such states will be published elsewhere. It should be noted that, depending on the sign of $E - E'$ in Eq. (A11), the frequency may be enhanced as well as reduced. For the considered Γ_6 state, the reduction frequency takes place because the Γ_6 one is below the group of remaining interacting states.

APPENDIX B: ADIABATIC POTENTIAL ENERGY SURFACES OF THE ${}^4T_1(F)$ STATE

Electronic operators $\mathcal{E}_\theta$ and $\mathcal{E}_\epsilon$ describing interaction of ${}^4T_1$ multiplet with E mode are calculated (as described in Sec. V A) in the base of six spin-orbit functions of this multiplet. The operators $\mathcal{E}_\theta$ and $\mathcal{E}_\epsilon$ are as follows:

$$\mathcal{E}_\theta = \begin{array}{c} \\ \Gamma_{6-1/2} \\ \Gamma_{8-1/2} \\ \Gamma'_{8-1/2} \\ \Gamma_{7-1/2} \\ \Gamma_{8\,3/2} \\ \Gamma'_{8\,3/2} \end{array} \begin{array}{c} \begin{array}{cccccc} \Gamma_{6-1/2} & \Gamma_{8-1/2} & \Gamma'_{8-1/2} & \Gamma_{7-1/2} & \Gamma_{8\,3/2} & \Gamma'_{8\,3/2} \end{array} \\ \begin{pmatrix} 0 & -\sqrt{5} & -3\sqrt{5} & 0 & 0 & 0 \\ -\sqrt{5} & 4 & -3 & 0 & 0 & 0 \\ -3\sqrt{5} & -3 & -4 & 0 & 0 & 0 \\ 0 & 0 & 0 & 0 & 3\sqrt{5} & -\sqrt{5} \\ 0 & 0 & 0 & 3\sqrt{5} & -4 & 3 \\ 0 & 0 & 0 & -\sqrt{5} & 3 & 4 \end{pmatrix} \end{array} \times \frac{1}{10} , \tag{B1}$$

$$\mathcal{E}_\epsilon = \begin{array}{c} \\ \Gamma_{6-1/2} \\ \Gamma_{8-1/2} \\ \Gamma'_{8-1/2} \\ \Gamma_{7-1/2} \\ \Gamma_{8\,3/2} \\ \Gamma'_{8\,3/2} \end{array} \begin{array}{c} \begin{array}{cccccc} \Gamma_{6-1/2} & \Gamma_{8-1/2} & \Gamma'_{8-1/2} & \Gamma_{7-1/2} & \Gamma_{8\,3/2} & \Gamma'_{8\,3/2} \end{array} \\ \begin{pmatrix} 0 & 0 & 0 & 0 & -\sqrt{5} & -3\sqrt{5} \\ 0 & 0 & 0 & -3\sqrt{5} & -4 & 3 \\ 0 & 0 & 0 & \sqrt{5} & 3 & 4 \\ 0 & -3\sqrt{5} & \sqrt{5} & 0 & 0 & 0 \\ -\sqrt{5} & -4 & 3 & 0 & 0 & 0 \\ -3\sqrt{5} & 3 & 4 & 0 & 0 & 0 \end{pmatrix} \end{array} \times \frac{1}{10} . \tag{B2}$$

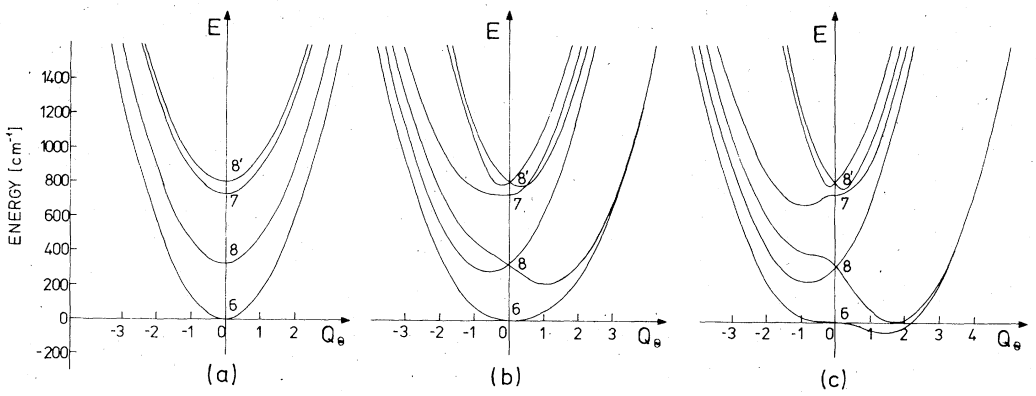

FIG. 13. Cross sections along the Q_θ axis of adiabatic potential energy surfaces of the $^4T_1(F)$ term for $\zeta = 385$ cm^{-1} and $\hbar\omega = 72$ cm^{-1} and for (a) $E_{JT} = 0$, (b) $E_{JT} = 200$ cm^{-1}, (c) $E_{JT} = 450$ cm^{-1}. The unit in the abscissa is $(\hbar/m\omega)^{1/2}$.

In the base of 12 wave functions of $^4T_1$ multiplet, the $\mathcal{E}_\theta$ and $\mathcal{E}_\epsilon$ operators should be matrices of 12×12 dimensions. However, because of Kramers degeneracy, the $\mathcal{E}_\theta$ and $\mathcal{E}_\epsilon$ matrices are the same in the base of the other six $\Gamma_{6\,1/2}, \Gamma_{8\,1/2}, \Gamma'_{8\,1/2}$, $\Gamma_{7\,1/2}, \Gamma_{8\,-3/2}, \Gamma'_{8\,-3/2}$ wave functions of $^4T_1$ multiplet.

Taking the momenta connected with Q_θ and Q_ϵ coordinates equal to zero in the full JT Hamiltonian $\mathcal{H} = \mathcal{H}_{so} + \mathcal{H}_{latt} + \mathcal{H}_{JT}$, one obtains an equation for potential energy of the system in the Γ_6, Γ_8, Γ'_8, and Γ_7 electronic states as a function of normal coordinates of the E mode. This equation has been solved by diagonalization of the 6×6 matrix Hamiltonian. The cross sections through adiabatic potential energy surfaces along Q_θ axis ($Q_\epsilon = 0$) for $E_{JT} = 0$, $E_{JT} = 200$ cm^{-1}, and $E_{JT} = 450$ cm^{-1} are shown in Fig. 13. Four paraboloids connected with Γ_6, Γ_8, Γ'_8, and Γ_7 electronic states, centered at $Q_\theta = 0$ and $Q_\epsilon = 0$, are obtained for $E_{JT} = 0$. It is seen from Figs. 13(b) and (c) that JT effect takes place only on Γ_8 states. The JT effect also introduces interaction between Γ_8 and Kramers doublet Γ_6 states. Therefore, the splitting of Γ_8 surface affects the lowest Γ_6 one. The Γ_6 surface is pushed apart and down by the Γ_8 one as JT energy is increased. The widening of the Γ_6 paraboloid causes the depression of vibronic levels; it is a well-known effect that vibronic levels become more closely spaced when the paraboloid is widened.

TABLE I. Reduced matrix elements $\langle \Gamma \| \mathcal{E}(\bar{\Gamma}) \| \Gamma' \rangle$ for $\Gamma = \Gamma_6$ electronic state of the $^4T_1$ multiplet for E and T_2 mode.

$\bar{\Gamma}$ \ Γ'	Γ_7	Γ_8	Γ'_8
$\Gamma_3(E)$	0	$-1/\sqrt{5}$	$-3/\sqrt{5}$
$\Gamma_5(T_2)$	$-\sqrt{2}$	$\sqrt{2}/\sqrt{5}$	$-2\sqrt{2}/\sqrt{5}$

The effect discussed above leads to local softening of the crystal around the cobalt impurity in the $^4T_1(F)$ state. Therefore, the effect of depression of vibronic levels, obtained from complex numerical calculations, has a very simple explanation.

The upper paraboloids connected with Γ_7 and Γ'_8 electronic states are narrowing, but the separation of them from the lowest Γ_6 one is not essentially affected by JT interaction. This is because the energy of the JT active mode $\hbar\omega$ is small compared to the full spin-orbit splitting of the

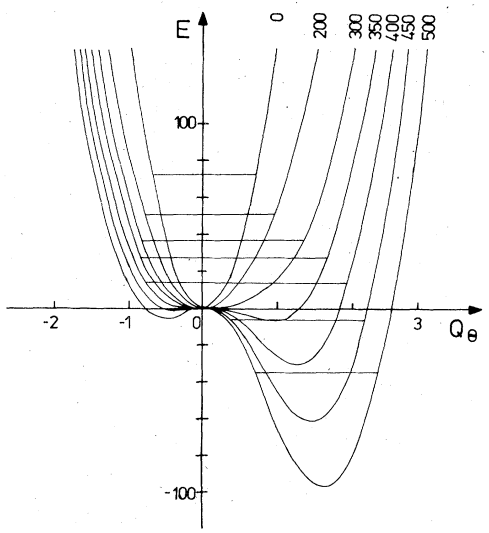

FIG. 14. Cross sections along the Q_θ axis of adiabatic potential energy surfaces of the lowest Γ_6 electronic state of the $^4T_1(F)$ term for increasing JT energies from 0 to 500 cm^{-1} ($\zeta = 385$ cm^{-1}, $\hbar\omega = 72$ cm^{-1}). The calculated positions of the lowest vibronic level in the potential minima are indicated. The unit in the abscissa is $(\hbar/m\omega)^{1/2}$, and in the ordinate cm^{-1}.

$^4T_1(F)$ term.

The cross sections through the Γ_6 potential energy surfaces for different E_{JT} are shown in Fig. 14. The positions of the lowest vibronic level, obtained from numerical calculations of the full Hamiltonian, are also indicated. The creation of static distortion is due to pushing down the Γ_6 sheet by the Γ_8. The static distortion takes place at about $E_{JT} = 440$ cm^{-1}. The three equivalent valleys in the Q_θ and Q_ϵ space are created (the cross section through only one of them is shown in Fig. 14). Therefore, for the static JT effect due to coupling to E mode, the lowest vibronic state should be of threefold orbital degeneracy (or sixfold, when spin is taken into account). This indeed takes place for $E_{JT} > 500$ cm^{-1} when the lowest Γ_6 and Γ_8 vibronic states merge together as is seen in Fig. 3. The small splitting between Γ_6 and Γ_8 levels, which still exists for E_{JT} between 440 and about 500 cm^{-1}, is due to tunneling effect. The barrier between valleys is so small that the system can tunnel from one valley to another. For sufficiently high E_{JT}, the system becomes frozen in one of the minima.

[1]F. S. Ham, Phys. Rev. 138, A1727 (1965).
[2]M. D. Sturge, Phys. Rev. B 1, 1005 (1970).
[3]M. D. Sturge and H. J. Guggenheim, Phys. Rev. B 4, 2092 (1971).
[4]P. Koidl, Phys. Status Solidi B 74, 477 (1976).
[5]F. S. Ham, W. M. Schwarz, and M. C. M. O'Brien, Phys. Rev. 185, 548 (1969).
[6]F. S. Ham and G. A. Slack, Phys. Rev. B 4, 777 (1971).
[7]S. Wittekoek, R. P. van Stapele, and A. W. J. Wijma, Phys. Rev. B 7, 1667 (1973).
[8]T. Yamaguchi and H. Kamimura, J. Phys. Soc. Jpn. 33, 953 (1972).
[9]P. Koidl, O. F. Schirmer, and U. Kaufmann, Phys. Rev. B 8, 4926 (1973).
[10]A. I. Ryskin, A. L. Natadze, S. A. Kazanskij, Zh. Eksp. Teor. Fiz. 64, 910 (1973) [Sov. Phys.-JETP 37, 462 (1973)].
[11]U. G. Kaufmann and P. Koidl, J. Phys. C 7, 791 (1974).
[12]H. Maier and U. Scherz, Phys. Status Solidi B 62, 153 (1974).
[13]U. Sauer, U. Scherz, and H. Maier, Phys. Status Solidi B 62, K71 (1974).
[14]R. Pappalardo and R. E. Dietz, Phys. Rev. 123, 1188 (1961).
[15]H. A. Weakliem, J. Chem. Phys. 36, 2117 (1962).
[16]J. M. Baranowski, J. W. Allen, and G. L. Pearson, Phys. Rev. 160, 627 (1967).
[17]J. M. Langer and J. M. Baranowski, Phys. Status Solidi B 44, 155 (1971).
[18]E. M. Wray and J. W. Allen, J. Phys. C 4, 512 (1971).
[19]K. K. Dubenskij, Y. E. Kariss, A. I. Ryskin, P. P. Feofilov, and G. I. Khil'ko, Opt. Spektrosk. 19, 635 (1965) [Opt. Spectrosc. 19, 353 (1965)].
[20]S. A. Kazanskij, A. I. Ryskin, and G. I. Khil'ko, Fiz. Tverd. Tela 10, 2415 (1968) [Sov. Phys.-Solid State 10, 1899 (1969)].
[21]P. Koidl and A. Räuber, J. Phys. Chem. Solids 35, 1061 (1974)
[22]J. W. Allen, Proc. Phys. Soc. Lond. 80, 1385 (1962).
[23]H. E. Gumlich and H. J. Schultz, J. Phys. Chem. Solids 27, 187 (1966).
[24]D. H. Loescher, J. W. Allen, and G. L. Pearson, J. Phys. Soc. Jpn. Suppl. 21, 239 (1966).
[25]J. M. Baranowski, M. Grynberg, and E. Magerramov, Phys. Status Solidi B 50, 433 (1972).
[26]B. R. Judd, *Operator Techniques in Atomic Spectroscopy* (McGraw-Hill, New York, 1963).
[27]B. G. Wybourne, *Spectroscopic Properties of Rare Earths* (Interscience, New York, 1965).
[28]C. W. Nielson and G. F. Koster, *Spectroscopic Coefficients for p^n, d^n, and f^n Configurations* (MIT, Cambridge, Mass., 1963).
[29]M. Rotenberg, R. Bivins, N. Metropolis, and J. K. Wooten, *The 3-j and 6-j Symbols* (MIT, Cambridge, Mass., 1959).
[30]E. U. Condon and G. H. Shortley, *Theory of Atomic Spectra* (Cambridge University, New York, 1935).
[31]G. Racah, Phys. Rev. 62, 438 (1942).
[32]It is important that relative phases of matrix elements of spin-orbit and crystal-field interaction should be consistent. They were taken as in Refs. 26 and 35, respectively.
[33]W. A. Runciman and K. A. Schroeder, Proc. R. Soc. A 265, 489 (1962).
[34]S. Sugano, Y. Tanabe, and H. Kamimura, *Multiplets of Transition-Metal Ions in Crystals* (Academic, New York, 1970).
[35]B. R. Judd, Phys. Rev. 127, 750 (1962).
[36]J. C. Irvin and J. La Combe, Can. J. Phys. 50, 2596 (1972).
[37]K. Kunc, M. Balkanski, and M. A. Nusimovici, Phys. Status Solidi B 72, 229 (1975).
[38]B. Hennion, F. Moussa, G. Pepy, and K. Kunc, Phys. Lett. A 36, 376 (1971).
[39]G. A. Slack and S. Roberts, Phys. Rev. B 3, 2613 (1971).
[40]A. Hadni, J. Claudel, and P. Strimer, Phys. Status Solidi 26, 241 (1968).
[41]S. S. Mitra, J. Phys. Soc. Jpn. Suppl. 21, 61 (1966).
[42]J. Vallin, G. A. Slack, S. Roberts, and A. E. Hughes, Phys. Rev. B 2, 4313 (1970).
[43]J. M. Baranowski, J. M. Noras, and J. W. Allen, *Proceedings of the Twelfth International Conference on Physics of Semiconductors, Stuttgart, 1974* (Teubner, Stuttgart, 1974), p. 416.
[44]S. Ushioda, A. Pinczuk, W. Taylor, and E. Burnstein, in *International Conference on II-VI Semiconducting Compounds*, edited by D. G. Thomas (Benjamin, New York, 1967), p. 1185.
[45]M. Krauzman, C. R. Acad. Sci. B 264, 1117 (1967).
[46]O. Brafman, I. F. Chang, G. Lengyel, S. S. Mitra, and E. Carnall, Jr., Phys. Rev. Lett. 19, 1120 (1967).
[47]W. Taylor, Phys. Lett. A 24, 556 (1967).
[48]W. G. Nilsen, in *Light Scattering Spectra of Solids*,

edited by G. B. Wright (Springer, New York, 1969), p. 129.
[49]R. Loudon, Proc. Phys. Soc. Lond. 84, 379 (1964).
[50]J. Kanamori, Prog. Theor. Phys. 17, 177 (1957).
[51]W. Moffit and W. Thorson, Phys. Rev. 108, 1251 (1957).
[52]G. F. Koster, J. O. Dimmock, R. G. Wheeler, and H. Statz, *Properties of the Thirty-Two Point Groups* (MIT, Cambridge, Mass., 1963).
[53]L. Pauling and E. B. Wilson, *Introduction to Quantum Mechanics* (McGraw-Hill, New York, 1935).
[54]H. C. Longuet-Higgins, U. Öpik, M. H. L. Pryce, and R. A. Sack, Proc. R. Soc. A 244, 1 (1958).
[55]*Quantum Theory*, edited by D. R. Bates (Academic, New York, 1961).
[56]S. L. Altmann and A. P. Cracknell, Rev. Mod. Phys. 37, 19 (1965).
[57]S. M. Uba (unpublished).
[58]This is due to the oscillator selection rules for matrix elements of the Jahn-Teller Hamiltonian linear in normal coordinates. For oscillator wave functions in the polar coordinates, these selection rules are $|\Delta N| = 1$ and $|\Delta m| = 1$ for E-mode, and $|\Delta N| = 1$ and $|\Delta l| = 1$ for T_2-mode, respectively (here l is the orbital quantum number of the three-dimensional oscillator).
[59]J. H. Wilkinson and C. Reinsch, *Handbook for Automatic Computation: Linear Algebra* (Springer, Berlin, 1971), Vol. II.
[60]A. V. Vasil'ev, A. L. Natadze, and A. I. Ryskin, Pis'ma Zh. Eksp. Teor. Fiz. 22, 43 (1975) [JETP Lett. 22, 19 (1975)].
[61]C. H. Henry, S. E. Schnatterly, and C. P. Slichter, Phys. Rev. 137, A583 (1965).
[62]F. S. Ham and V. Grevsmuhl, Phys. Rev. B 8, 2945 (1973).